Chapter 11

Extratropical Cloud Systems and Cloud Radiative Forcing

C.P. Weaver and V. Ramanathan

Center for Atmospheric Sciences and Center for Clouds, Chemistry and Climate, Scripps Institution of Oceanography, UCSD, La Jolla, USA.

Abstract

Recent satellite observations have shown that extratropical oceanic clouds have the largest magnitude net (longwave plus shortwave) cloud radiative forcing (CRF) of any global cloud system. These clouds are responsible for approximately 50% of the net, annual-mean cloud cooling effect on the global, top-of-atmosphere radiation budget. The observations further suggest that variations in large-scale CRF depend on variations in vertical velocity and low-level static stability on timescales ranging from daily to monthly. The nature of the dependence of CRF on given dynamical and thermodynamical parameters suggests that it is instructive to separate the contribution to total column CRF by low-level clouds (controlled largely by boundary layer processes) and clouds at higher levels (strongly influenced by large-scale ascent and descent associated with extratropical cyclones). It is concluded that low- and high-level clouds both play an important role in determining the large magnitude shortwave CRF in the Northern Hemisphere oceanic storm tracks.

1 Introduction

Research into clouds and cloud processes is important both because clouds are a strong determinant of the current global climate, and because clouds interact in complex ways with other components of the climate system, leading to the possibility of climate change feedbacks. Currently, however, the inaccurate parameterization of clouds impacts many aspects of model-simulated climate (Gleckler et al., 1995; Kiehl et al., 1995) and also produces the largest uncertainty in model response to climate forcing (Cess et al., 1990). This paper discusses the important role of extratropical oceanic clouds in the global

radiation budget, and presents observational results which illustrate fundamental links between these clouds and the large-scale atmospheric dynamics and thermodynamics.

Clouds influence the Earth's radiation budget by interacting with the longwave (terrestrial) and shortwave (solar) fluxes. This impact is termed cloud radiative forcing (CRF), and it is an important term in the Earth's energy balance. The results discussed in this paper are drawn largely from Weaver (1996), Weaver and Ramanathan (1996) and Weaver and Ramanathan (1997). We examine the role NH extratropical oceanic cyclones play in determining cloudiness and CRF, the critical importance of boundary-layer clouds, and how large-scale vertical velocity and static stability influence CRF in a given region and season. We focus mainly on summer, since this is when extratropical clouds have the largest impact on the global radiation budget at the top of the atmosphere, but we also discuss wintertime. The basic conceptual model put forth in this paper to explain the distribution of cloudiness and CRF in the NH oceanic storm track regions is as follows: to first order, cyclones and other synoptic-scale weather disturbances provide large-scale vertical motions which strongly influence CRF above the boundary layer (due to mid- and upper-level cloud formation). Within the boundary layer, cloud cover (and hence CRF), is a function of boundary layer thermodynamic structure as diagnosed by parameters such as static stability. While clouds in the free troposphere have potentially much greater vertical extents than boundary layer clouds, the radiative properties of both classes are such that both are important in determining the overall storm track CRF.

The conceptual model has been developed by examining the differences in cloud cover and CRF between and within the North Pacific and North Atlantic during a given season, and between winter and summer within a given ocean basin. For example, Table 1 shows total cloud amount (TCA) for winter (DJF) and summer (JJA) in the North Pacific and North Atlantic. While wintertime TCA is approximately the same for both oceans, summertime TCA is much greater in the Pacific (86.6 %) than in the Atlantic (71.1 %). Is this difference reflected in the seasonality of the basic meteorology and climatology of each region? Section 2 discusses CRF definitions and observations. Section 3 presents results demonstrating the link between extratropical synoptic-scale dynamics and CRF, while Section 4 focuses on low-level clouds and their important radiative influence. Section 5 discusses regional and seasonal CRF variations, and Section 6 provides a summary and discussion.

Table 1. Warren et al. : 1988 total cloud amount (TCA; %) for selected regions.

Basin	DJF	JJA
N. Pacific (lat 35-60°N, lon 160-220°)	78.0	86.6
N. Atlantic (lat 35-60°N, lon 310-350°)	77.4	71.1

2 Cloud radiative forcing (CRF)

2.1 Definitions and data

NASA's Earth Radiation Budget Experiment (ERBE) (see Barkstrom, 1984) used satellite observations to infer the role of clouds in the radiation budget at the top of the atmosphere (Ramanathan et al., 1989). By identifying clear and cloudy scenes, ERBE produced estimates of CRF, which can be divided into longwave (C_l) and shortwave (C_s) components. C_l is defined as follows:

$$C_l = F_c - F \ . \tag{1}$$

F_c is clear-sky outgoing longwave radiation (OLR), while F is OLR for mean cloudy conditions (mixed clear and cloudy skies). Since clouds tend to reduce the OLR of the planet (i.e. they enhance the greenhouse effect), C_l is generally positive. Clouds also tend to increase the Earth's albedo, decreasing the solar heating. C_s is therefore defined as:

$$C_s = S(1 - A) - S_c \ . \tag{2}$$

S is the solar insolation at the top of the atmosphere, A is the column albedo, and S_c is the total clear-sky solar absorption. According to this definition, C_s is generally negative.

Much of the analysis summarized in this paper uses the following ERBE data: Monthly-mean ERBE C_s and C_l data for January and July 1985-89 on a global 2.5° by 2.5° grid; and daily-mean C_s and C_l (for the same time period and at the same resolution) computed by differencing the daily ERBE clear and cloudy OLR and outgoing solar radiation values, when available, or by differencing the daily cloudy values and monthly-mean clear values when clear-sky values are unavailable for a given day. A more detailed description of this data can be found in Ramanathan et al. (1989) and Harrison et al. (1990).

A large part of the seasonal variation in C_s is due to changes in insolation rather than cloud properties (Cess et al., 1992). In order to directly compare ERBE data from January and July in some of our analysis, C_s has been normalized by a factor (f) which is proportional to diurnal-mean insolation at each point (e.g. see Fig. 6.4 and Eq. 6.13-18 in Peixoto and Oort, 1992). This normalized C_s, or C_{sn}, is defined such that $C_{sn} = C_s/f$. This factor accounts for variation in Earth-Sun distance, solar declination, and latitude. It does not take into account the fact that total albedo and clear-sky albedo may have systematically different responses to seasonal solar zenith angle variations. Simulations using a simple radiative transfer code indicate,

however, that this effect introduces limited variability into C_{sn}.

In addition to the ERBE data, the results presented in this paper draw from several other data sets. The Warren et al. (1988) cloud atlas provides a ship-based climatology of cloud type observations over the ocean during the period December 1951 to November 1981. This atlas consolidates daily and hourly Comprehensive Ocean-Atmosphere Data Set (COADS) observations in monthly and seasonal climatologies of cloud frequency of occurrence, cloud amount when present, and total cloud amount. Warren et al. (1988) uses the following definitions for the cloud type amounts which we present here: St (stratus + stratocumulus + fog); As (altostratus + altocumulus); Ns (nimbostratus); Cu (cumulus); Cb (cumulonimbus). More detailed information about these observations can be found in the land and ocean atlases (Warren et al., 1986; Warren et al., 1988). ECMWF analyzed fields from the World Meteorological Organization (WMO) archive provide various meteorological variables on seven pressure levels (1000, 850, 700, 500, 300, 200 and 100 mb) (Trenberth and Olson, 1988a; Trenberth and Olson, 1988b). Finally, we also briefly examine radiosonde temperature and humidity profiles taken from the National Meteorological Center for Environment Prediction (NCEP) ship sounding database.

2.2 Observations

While clouds have both heating (C_l) and cooling (C_s) influences, global mean net ERBE CRF ($C_l + C_s$) is roughly -15 to -20 $W\,m^{-2}$ (Ramanathan et al., 1989; Harrison et al., 1990). In other words, the magnitude of C_s (45 to 50 $W\,m^{-2}$) exceeds that of C_l (approximately 30 $W\,m^{-2}$), and clouds have a net radiative cooling effect on the planet. Looking at a daily satellite image of the globe, one realizes that clouds are present in the extratropical regions to a large extent throughout the year, often as comma- and spiral-shaped structures associated with cyclonic disturbances. Since the horizontal scale of these systems is often greater than 1000 kilometers, it is reasonable to infer that they might have a significant impact on the Earth's radiation budget. Harrison et al. (1990) investigated the regional and seasonal distribution of CRF and found that, while the magnitudes of C_s and C_l can be individually large in given regions and seasons, only over the extratropical and subtropical oceans during the warm season does the magnitude of C_s significantly exceed that of C_l. This large negative contribution dominates the observed global and annual average cloud radiative cooling. Fig. 1 shows maps of five-year mean (1985-89) Northern and Southern Hemisphere (NH and SH) C_s, illustrating the strong signal of extratropical oceanic clouds (light shading indicates large magnitude C_s). C_s is highly seasonal, varying with insolation changes, and during summer, the magnitude of monthly-mean C_s can exceed that of C_l by more than 100 $W\,m^{-2}$. Using the ERBE data, we estimate that oceanic

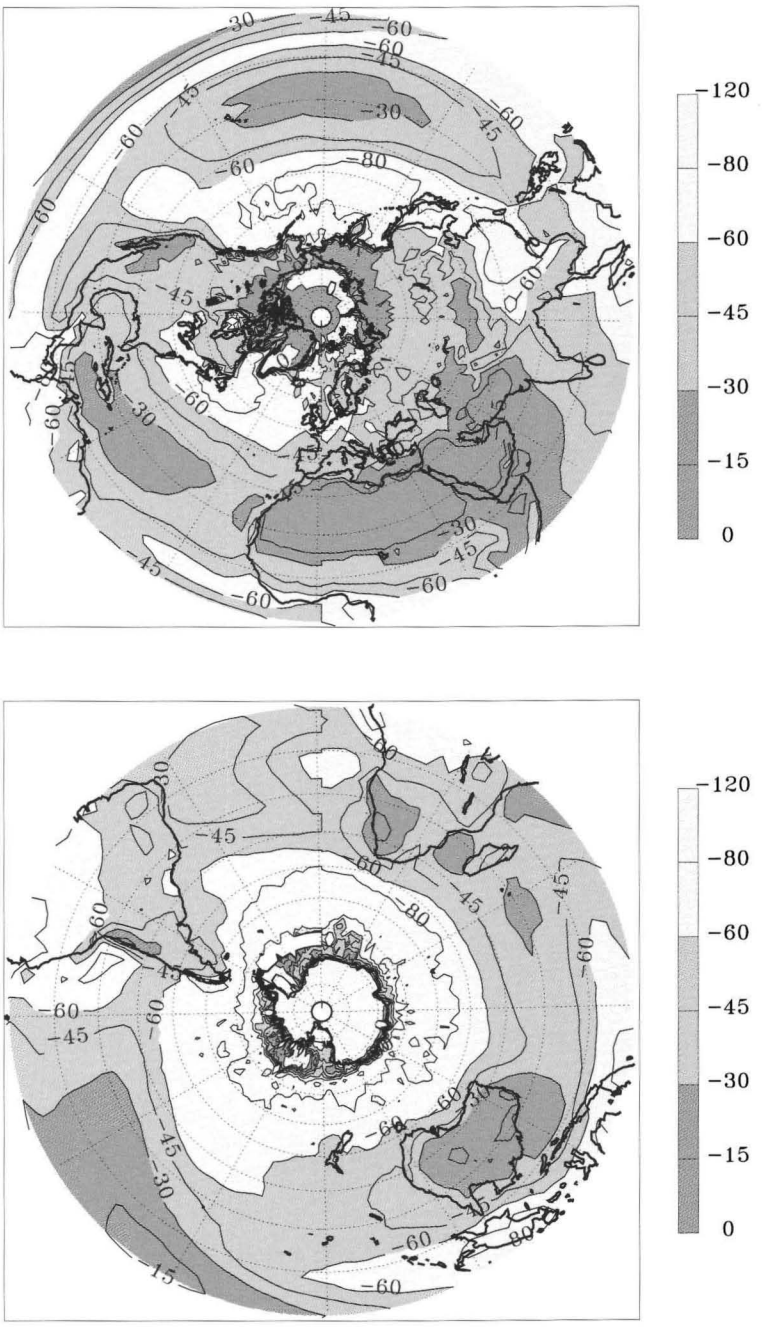

Fig. 1. 1985-89 Mean ERBE C_s ($W\,m^{-2}$) (Weaver and Ramanathan, 1996).

clouds between 35° and 70° latitude in both hemispheres contribute approximately 50% to the globally and annually averaged net CRF. Thus we can conclude that the amount of energy modulated by extratropical oceanic cloud systems is large from a climate forcing perspective (Ramanathan, 1995) and can potentially influence dynamical processes in the atmosphere and ocean through their respective energy budgets (Gleckler et al., 1995; Weaver, 1996). Fig. 1 demonstrates the geographic correspondence between the peak C_s values and the midlatitude storm tracks. While it has long been recognized that clouds and precipitation in the extratropics are closely linked to large-scale atmospheric motions within cyclones and other weather phenomena (Palmen and Newton, 1969; Petterssen, 1969; Wallace and Hobbs, 1977; Holton, 1992), there has been relatively little research into the relationships between extratropical dynamics and thermodynamics and CRF. Because of the paramount importance of extratropical oceanic clouds in the radiation budget, research into the physical mechanisms which control CRF in these regions is a necessary prerequisite for improving the representation of clouds in models and accurately simulating climate and climate change.

Here we briefly summarize some recent work relating to these issues. Sheu and Curry (1992) compare the U.S. Air Force Three-Dimensional Nephanalysis with heat and moisture budgets computed from ECMWF analyzed fields for the midlatitude North Atlantic during January. They conclude that mid-level clouds form primarily due to large-scale three-dimensional moisture convergence, while low clouds depend on surface moisture flux and static stability. Klein and Hartmann (1993) use data from the Warren et al. (1988) oceanic cloud atlas in conjunction with ECMWF analyzed fields to investigate the seasonal cycle of low stratiform clouds in the subtropics and extratropics. They find that low stratiform cloud fraction is a robust function of lower troposphere static stability, with increases in static stability associated with increases in cloud fraction. Norris and Leovy (1994) find that marine stratiform cloudiness is significantly anti-correlated (on an interannual basis) with sea-surface temperature (SST) anomalies over extratropical and eastern subtropical oceans. They also report an anti-correlation between extratropical SST and nimbostratus and non-precipitating mid-level clouds, which they attribute to displacement of the storm tracks over regions of negative SST anomalies. Lau and Crane (1995) examine International Satellite Cloud Climatology Project (ISCCP) data in the context of the North and South Atlantic wintertime storm track dynamics. They show that the patterns of satellite-inferred optical depths are consistent with accepted ideas about cloud organization, structure and properties within extratropical cyclones.

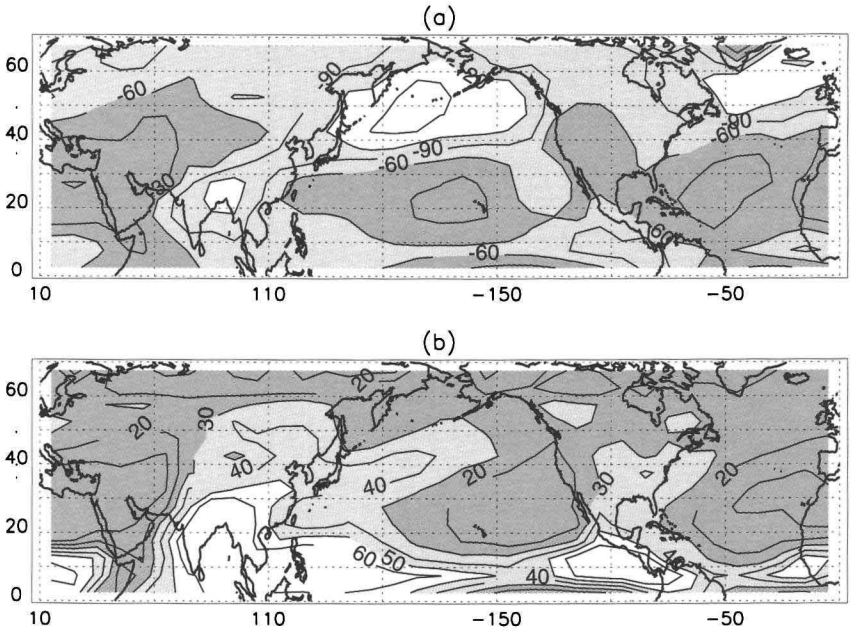

Fig. 2. (a) July 1985-89 ERBE C_s and (b) July 1985-89 ERBE C_l ($W\,m^{-2}$).

3 Cloud radiative forcing and extratropical clouds

Let us focus more closely on C_s and C_l over the NH oceans during July (Fig. 2). The mean July 1985-89 magnitude of C_s is large in the storm tracks over the North Pacific and North Atlantic, with values exceeding -150 $W\,m^{-2}$ over the North Pacific. C_l also increases in the storm tracks relative to the subtropics, averaging approximately 30 $W\,m^{-2}$. As noted in Section 1, net CRF is strongly negative, and clouds are cooling the extratropical North Pacific and North Atlantic during July. The positions of the July maxima in extratropical oceanic C_s coincide with the summertime maxima in St, As, and TCA from the Warren et al. cloud atlas (Table 3). As discussed in Weaver and Ramanathan (1996), the region of largest magnitude monthly-mean C_s is approximately the region of greatest overlap between low, middle and high clouds, and also the region of maximum ISCCP cloud optical depth.

Given that storm track cyclones are associated with extensive stratiform cloud systems and characterized by clouds at all levels of the troposphere, how does the short timescale phenomenon of traveling cyclones contribute to this longer-term mean CRF picture? Weaver and Ramanathan (1996) examine the simultaneous evolution of CRF and the ECMWF 1000 *mb* geopotential height

Table 2. Warren et al. : 1988 cloud type (%) and ERBE CRF ($W\,m^{-2}$).

	N. Pacific (lon 160-220°)			N. Atlantic (lon 310-350°)		
Quantity	35-40°N	40-50°N	50-60°N	35-40°N	40-50°N	50-60°N
			DJF 1952-81			
St	50.0	55.1	52.4	38.2	50.5	49.5
As	25.7	23.2	19.5	28.6	28.1	25.8
Ns	10.9	13.7	19.3	5.5	10.1	14.8
Cu	9.1	7.1	5.4	12.2	8.9	10.6
Cb	5.2	4.7	5.6	6.4	6.8	9.3
			January 1985-89			
C_s	-51	-39	-19	-40	-38	-21
C_{sn}	-114	-117	-111	-90	-116	-119
C_l	50	42	34	41	46	44
			JJA 1952-81			
St	51.2	78.4	73.8	24.1	50.0	63.7
As	29.8	40.9	33.8	17.1	26.3	30.1
Ns	7.3	10.5	12.7	2.0	6.4	12.4
Cu	8.7	2.3	2.4	15.3	7.8	4.4
Cb	3.5	1.3	1.1	4.8	3.3	2.9
			July 1985-89			
C_s	-93	-141	-140	-41	-86	-133
C_{sn}	-86	-131	-133	-38	-80	-127
C_l	32	34	27	13	22	27

field for July 1985 in order to track the contribution of cyclone clouds to the time-mean CRF field. Specifically, they identify the location of low centers from traveling cyclones for each day throughout the month. They show that the region of peak monthly-mean C_s magnitude is geographically co-located with the distribution of low centers to a high degree, and that this is consistent with the observed pattern of cyclogenesis off the Asian east coast and subsequent downstream evolution of the cyclones and their associated cloud systems. Weaver and Ramanathan (1996) conclude that clouds associated with

traveling cyclones are responsible for a significant fraction of the total North Pacific July C_s signal. Our first goal is therefore to link the CRF fields to the dynamical fields within individual cyclones. This provides a context for interpreting statistical or composite correlations between the satellite and meteorological data on daily- and monthly-mean timescales.

Fig. 3 presents a case study of a North Atlantic cyclonic storm on July 2, 1987. The 1000 *mb* geopotential height field (Fig. 3a) reveals a closed low just south of Greenland. A broad high dominates the southern and eastern part of the extratropical North Atlantic. This is the summertime northward extension of the climatological subtropical high. Cyclones in general are associated with

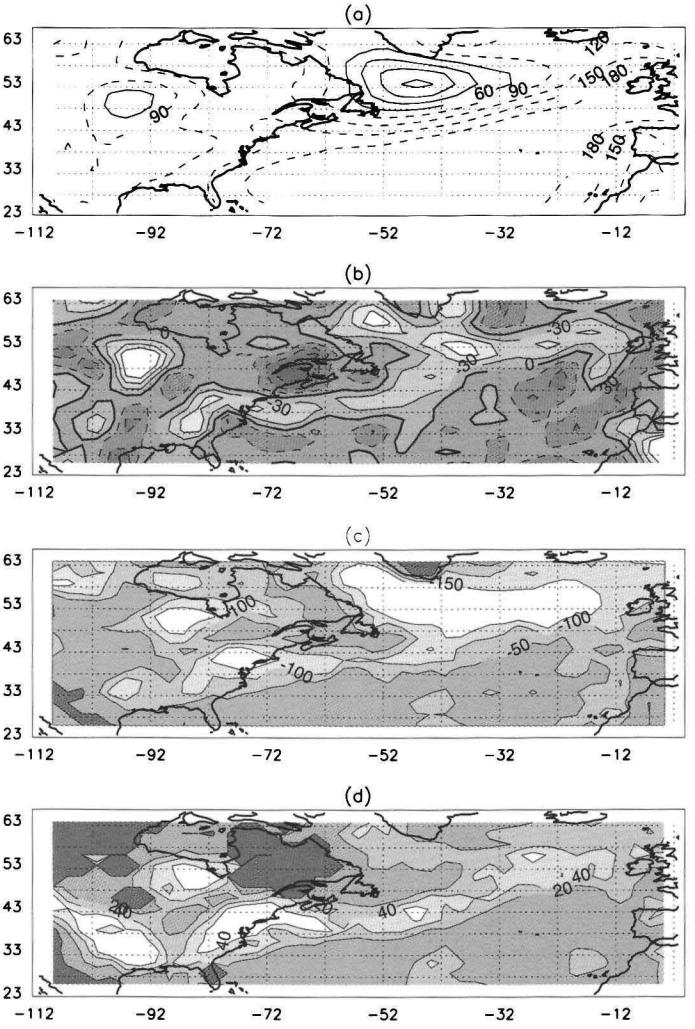

Fig. 3. ECMWF and ERBE fields for a North Atlantic case study cyclone (July 2, 1987). (a) ECMWF 1000 mb Z (m). (b) ECMWF 850 mb ω ($mb\,day^{-1}$). (c) ERBE C_{sn} ($W\,m^{-2}$). (d) ERBE C_l ($W\,m^{-2}$).

well-organized patterns of horizontal and vertical circulations. The horizontal winds (not shown) are approximately geostrophic, with counterclockwise circulation around the low. The 850 mb vertical pressure velocity (ω) map (Fig. 3b) shows strong rising motion (negative values; light shading and solid contours) in advance (eastward) of the low in the warm, poleward-moving airstream. Strong sinking motion (positive values; dark shading and dashed contours) is present behind (westward of) the low in the cold, equatorward-moving flow. This relationship of the vertical motion field to the surface geopotential and horizontal circulations (i.e. the positions of the warm and cold fronts) is what we expect from an extensive survey of synoptic-scale meteorology in the mid-latitudes (e.g. see Fig. 11.3 in Houze, 1993). We note that values of ω at a given level above the boundary layer tend to be representative of values anywhere in the free troposphere, because large-scale vertical motion associated with cyclones tends to extend throughout much of the column. A map of 500 mb ω, for example, would look very similar to the 850 mb map presented in Fig. 3b. The region of generally high geopotential to the south and east of the cyclone is characterized by relatively weaker but geographically more extensive subsidence, in accordance with our understanding of the climatology of subtropical and eastern extratropical ocean regions.

The ω field is closely associated with the CRF fields. The region of rising motion around the low corresponds to a geographically extensive and highly reflective cloud shield or band with C_{sn} < -150 $W\,m^{-2}$ (Fig. 3c), and these large magnitude C_{sn} values coincide, in part, with middle and high clouds with C_l > 40-60 $W\,m^{-2}$ (Fig. 3d). Peak C_s values in these summertime cyclone cloud shields can exceed -200 $W\,m^{-2}$. The region of sinking motion behind the low is characterized by smaller C_{sn} and C_l magnitudes (i.e. lower cloud tops and a less-reflective total cloud column). These results are consistent with the general conclusions of Lau and Crane (1995) and Weaver and Ramanathan (1997) regarding cloud organization within cyclones as inferred from satellite data and analyzed fields. Both studies considered composites of many systems rather than individual cases. It is interesting to note that, though it is perhaps unreasonable to expect the correspondence between two such different datasets (ERBE and ECMWF) to be perfect, dynamical features from the analyzed fields agree quite well with ERBE CRF on daily timescales. The subsidence associated with the subtropical high is associated with relatively smaller CRF magnitudes, indicating a regime which is also dominated by low clouds. This strong correspondence between the ω and CRF fields can be illustrated in a different way. Weaver and Ramanathan (1997) binned the daily-mean ERBE data by daily-mean ECMWF 500 mb ω (Fig. 4). Each value represents an area-weighted average in a 0.02 $Pa\,s^{-1}$ (or approximately 17 $mb\,day^{-1}$) bin for January and July 1985-89 in the North Pacific (lat 35°-60°N, lon 160°-220°) and North Atlantic (lat 35°-60°N, lon 310°-350°). Fig. 4a-b shows C_{sn} as a function of 500 mb ω, while Fig. 4c-d shows C_l. These figures show C_{sn} rather than C_s in order to facilitate a more direct comparison between January and July values (see Section 2.1).

Consistent with our preceeding discussion, rising motion ($\omega < 0$) is associated with thick cloud decks and high cloud tops (roughly 1-10 kilometer thick clouds with correspondingly large C_{sn} and C_l magnitudes), while sinking motion ($\omega > 0$) is associated with thinner cloud decks and low cloud tops (clouds are mostly confined to low levels of the troposphere and have smaller magnitude C_{sn} and C_l values). This behavior of C_{sn} and C_l vs. ω is qualitatively the same for all four cases considered (North Pacific January and July; North Atlantic January and July). The standard deviation for each bin is fairly large (approximately 40-60 $W\,m^{-2}$ for C_{sn}; approximately 15-20 $W\,m^{-2}$ for C_l as shown Fig. 4) indicating considerable scatter, though the

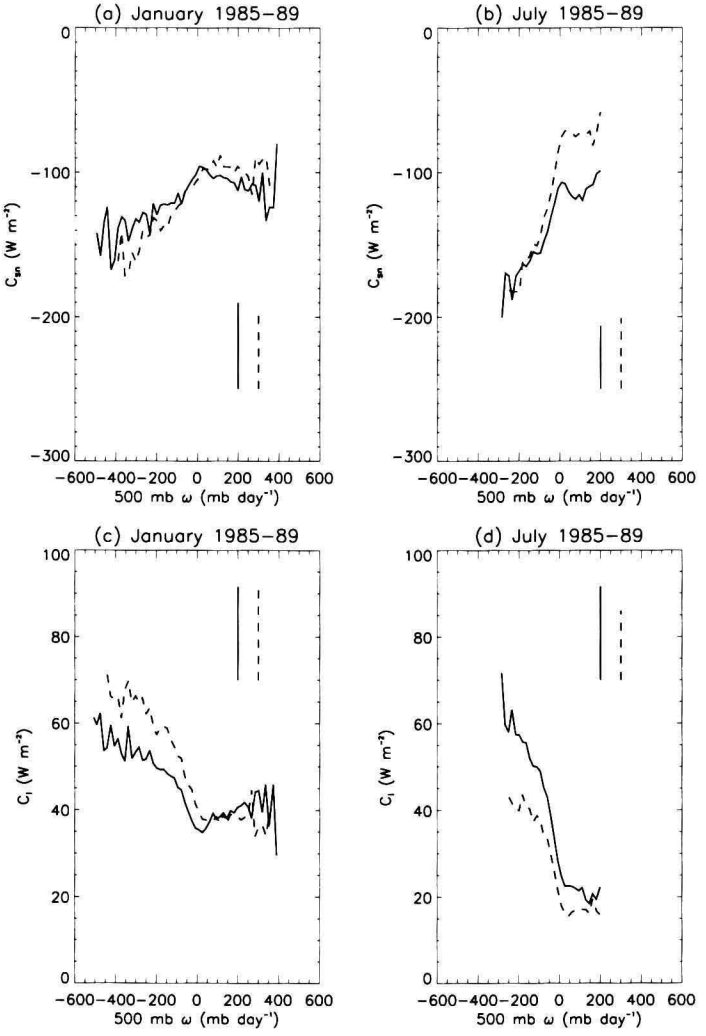

Fig. 4. ERBE C_{sn} binned by ECMWF 500 mb ω (dashed line is N. Atlantic, solid line is N. Pacific). Mean standard deviations are indicated by the vertical lines (from Weaver and Ramanathan, 1997).

number of points in each bin also tends to be large. Fig. 4 illustrates that the relationship between CRF and ω is quite different between rising and sinking regimes. Where $\omega < 0$, C_{sn} and C_l magnitudes increase approximately linearly with increasing intensity of rising motion. Where $\omega > 0$, however, C_{sn} and C_l magnitudes remain relatively constant (at minima) regardless of the intensity of sinking motion.

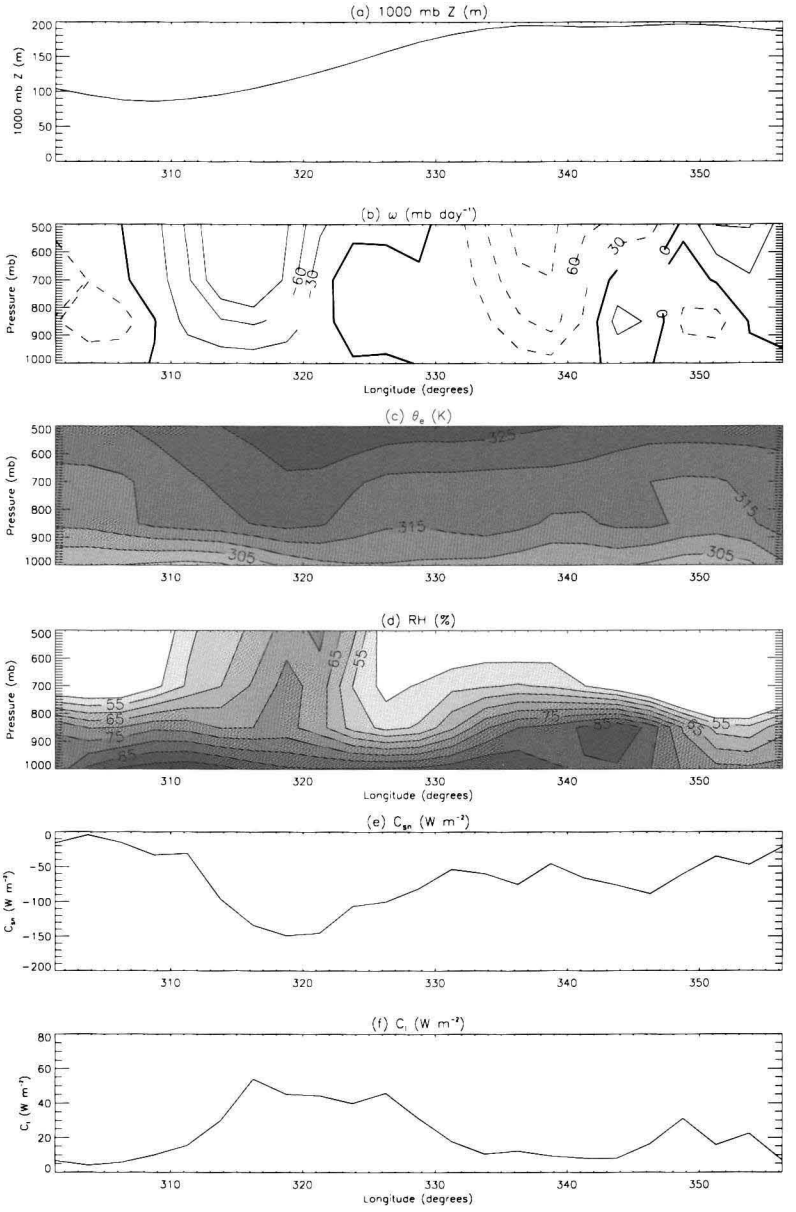

Fig. 5. ECMWF and ERBE fields in a vertical-longitude slice (at 46.25°N) through the July 2, 1987 case study cyclone of Fig. 3.

We interpret these results as follows: In regions of large-scale ascent, clouds are present throughout many vertical levels, and the thickest (and therefore most highly reflective) scenes are those where the most intense rising motion is occurring. Subsidence, on the other hand, suppresses middle and high cloud formation, leaving mostly low (boundary layer) clouds, and parameters besides ω play a more important role in determining cloudiness and hence CRF. Returning to our case study of Fig. 3, Fig. 5 further illustrates this interpretation of the influence of ω on CRF and the vertical distribution of cloud cover by showing a longitudinal-vertical cross-section through the cyclone (at $46.25°N$ latitude). The strong region of rising motion (solid contours in Fig. 5b) just to the east of the surface low is characterized by a significantly moister mid- and upper troposphere than the adjacent subsidence regions (Fig. 5d). Correspondingly, C_{sn} (Fig. 5e) and C_l (Fig. 5f) have pronounced peaks in the ascent region, with much smaller (and relatively constant) magnitudes elsewhere. The boundary layer is uniformly moist in both rising and sinking areas.

Thus, we consider a subsidence regime, dominated by boundary layer clouds and processes, and an ascent regime where large-scale rising motion 'dynamically' forces cloud formation above the low clouds already present. It is worthwhile to point out that, though the ascent regime (lower and upper level clouds combined) has larger magnitude C_{sn} values, low clouds in regions of subsidence can contribute on the order of -100 $W\,m^{-2}$ to the radiation budget at a given time (Fig. 4). Since it is clear that low-level clouds can play a significant radiative role in both regimes, it is important to investigate the factors which influence boundary layer cloudiness.

4 Low-level clouds and static stability

First, we present a simple, qualitative discussion of cloudy boundary layers over the extratropical oceans. One important point is that, over much of the NH extratropical and eastern subtropical oceans, temperature inversions are often present above the boundary layer. These inversion-capped boundary layers are frequently associated with stratus and stratocumulus clouds and have been relatively well-observed, particularly in the subsidence regimes of the subtropical high (Klein and Hartmann, 1993; Albrecht et al., 1995b; Betts et al., 1995). Above the inversion, potential temperature (θ) increases, and relative humidity and water vapor mixing ratio decrease sharply with altitude. Typical inversion altitudes are in the range 750-1500 meters. Below the inversion, there is a often slightly stratified cloud layer approximately 100-500 meters thick between the lifting condensation level and the inversion as well as a well-mixed subcloud layer (e.g. see Fig. 1 and 2 and Table 2 from Albrecht et al., 1995b).

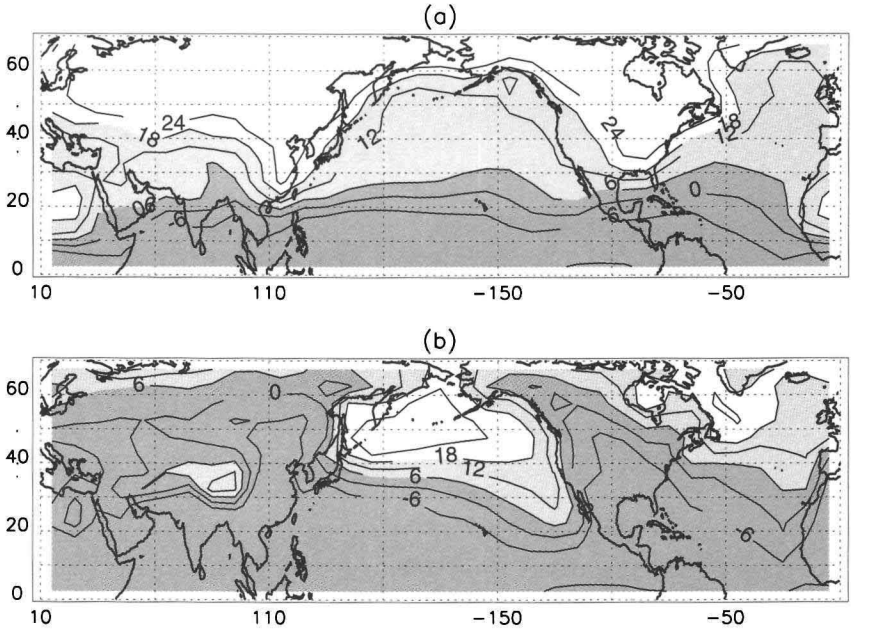

Fig. 6. (a) January 1985-89 and (b) July 1985-89 $700\,mb\,\theta_e - 1000\,mb\,\theta_e$ (K).

These inversions tend to occur under conditions of large-scale subsidence, particularly in the subtropics, and also due to the advection of warm air over relatively colder ocean (Klein and Hartmann, 1993). This tendency is most pronounced during summer, when inversions are more frequent and occur lower in the atmosphere, resulting in a shallower boundary layer and a more statically stable lower troposphere. Klein and Hartmann (1993) examine sounding data from weathership B in the North Atlantic ($57°N$, $51°W$ during the period 1949-1974) and find that 70% of July soundings have an inversion below 500 *mb*, and that the mean inversion base and top are 947 and 899 *mb*, respectively. By contrast, only 29% of January soundings have an inversion, and the mean inversion occurs higher in the atmosphere (base at 826 *mb* and top at 781 *mb*). When the ocean is relatively warm compared to the overlying air (e.g. during wintertime cold-air outbreaks following the passage of a cold front), the boundary layer is generally deeper and more convective, inversions are less frequent, and the lower troposphere is less statically stable (Klein and Hartmann, 1993; Weaver and Ramanathan, 1997).

Fig. 6 shows mean 1985-89 January and July climatologies of one approximate measure of low-level static stability, the difference in equivalent potential temperature (θ_e) between 700 and 1000 *mb* calculated from ECMWF temperatures and humidities. These maps clearly illustrate the seasonality of the lower-tropospheric thermodynamic structure; particularly striking is the pronounced increase in static stability from January to July over the North Pacific. Observations indicate that large-scale low-level static stability and large-scale low

cloud fraction are strongly related. Klein and Hartmann (1993) find a linear relationship between a different, but qualitatively similar, measure of static stability (700 $mb\,\theta$ - θ at the surface) and low stratiform cloud fraction over subtropical and midlatitude oceans, such that cloud fraction increases with increasing static stability. Weaver and Ramanathan (1997) show that climatological values of 500 $mb\,\theta_e$ – 1000 $mb\,\theta_e$ from the midlatitude North Pacific and North Atlantic during winter and summer are positively correlated with the climatologies of low stratiform cloud fraction from Warren et al. (1988) and negatively correlated with cumulus cloud fraction (Fig. 7). Though here we show θ_e differences between 500 and 1000 mb (rather than between some lower level and 1000 mb), the variation in this difference is dominated by variation in the low-level θ_e difference, and it is sufficient to choose a value of θ_e from somewhere in the free troposphere in order to capture the variability of low-level static stability (or, equivalently, inversion strength), reasonably well. As Fig. 7 (and also Table 3) indicates, a shift in the predominance of horizontally extensive stratiform clouds to horizontally limited cumuliform clouds with a shift in static stability leads to a smaller overall cloud fraction (Sellers, 1976).

Since we expect that greater low-level static stability implies greater low-level stratiform cloud cover, and hence total cloud fraction, we are interested in the effect this might have on CRF. In a similar fashion to Fig. 4, Weaver and Ramanathan (1997) show daily-mean C_{sn} and C_l binned by daily-mean

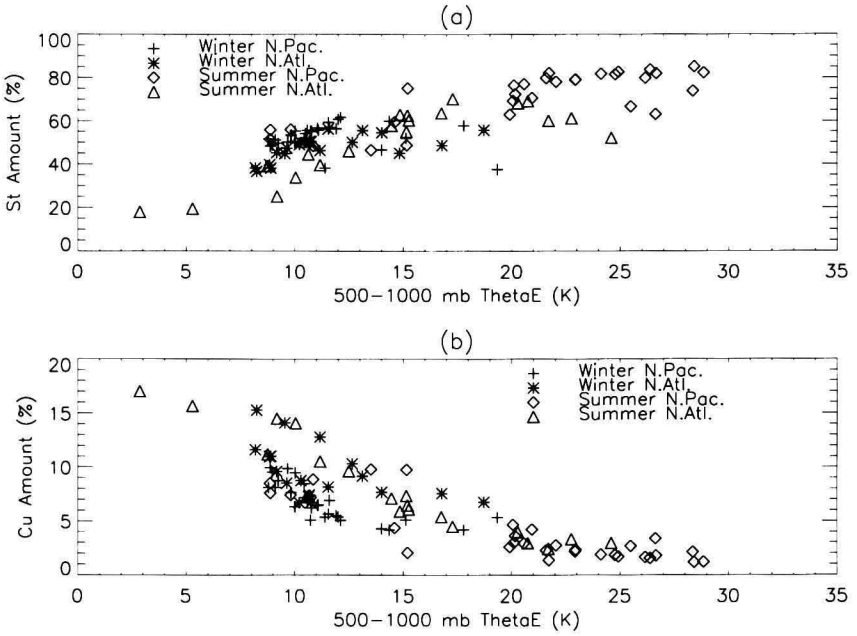

Fig. 7. Warren et al. : (1988) (a) St and (b) Cu climatological amount as a function of 500 $mb\,\theta_e$ – 1000 $mb\,\theta_e$ climatology (from Weaver and Ramanathan, 1997).

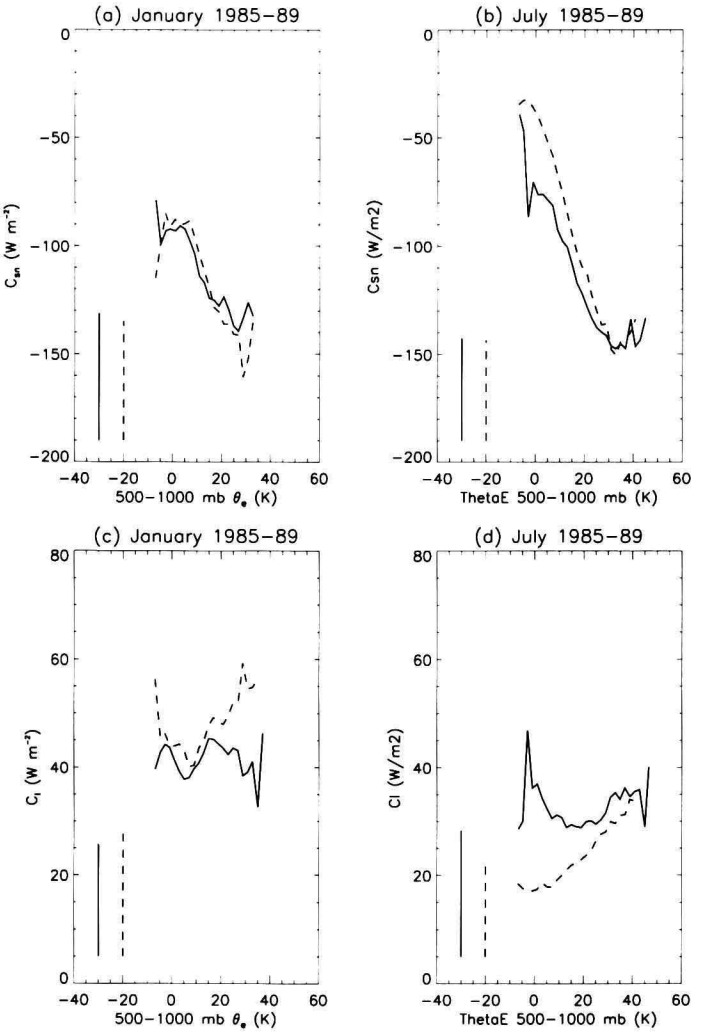

Fig. 8. ERBE C_{sn} and C_l binned by $500\,mb\,\theta_e - 1000\,mb\,\theta_e$ (see, e.g. Fig. 4) (from Weaver and Ramanathan, 1997).

$500\,mb\,\theta_e - 1000\,mb\,\theta_e$ (Fig. 8). Fig. 8 shows that the magnitude of C_{sn} increases with increasing static stability (Fig. 8a-b). By contrast, C_l doesn't vary with static stability in a coherent manner (Fig. 8c-d). Both these results are consistent with our expectation that low cloud fraction increases with increasing static stability, since, unlike the relationship between ω and CRF, C_{sn} varies without a corresponding variation in cloud top altitude. Weaver and Ramanathan (1997) find that this dependence of C_{sn} on static stability holds separately in regions of both rising and sinking motion. This is also consistent with the idea that the processes which control boundary layer cloud cover are similar regardless of the background meteorology (e.g. low cloud fraction responds to static stability behind a cold front or ahead of a warm front, in

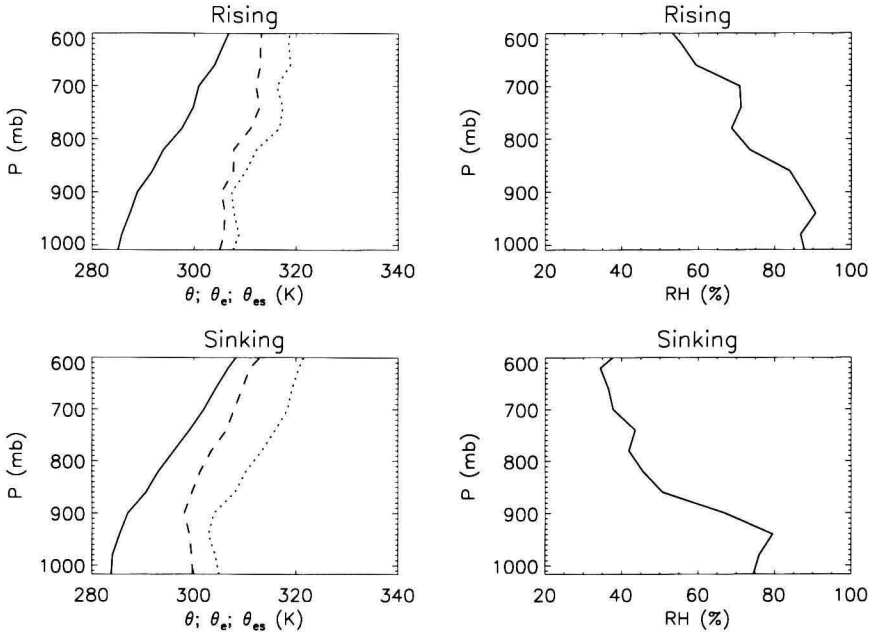

Fig. 9. Composite NMC ship soundings for rising motion (ECMWF 850 $mb\,\omega < -50$ $mb\,day^{-1}$) and sinking motion (ECMWF 850 $mb\,\omega > 50$ $mb\,day^{-1}$).

a cyclonic or anticyclonic regime, etc.) while cloudiness above the boundary layer varies.

Fig. 9 shows composite profiles of of θ, θ_e, θ_{es} (saturated equivalent potential temperature), and relative humidity constructed from NCEP ship soundings launched during the five Julys from 1985-89. We use North Atlantic soundings in the region 55-60°N latitude and longitude 310-350°. The top panels show a composite of soundings where there was strong rising motion present (ECMWF 850 $mb\ \omega < -50\ mb\,day^{-1}$; 55 soundings), and the bottom panels shows a composite where there was strong sinking motion present (ECMWF 850 $mb\ \omega > 50\ mb\,day^{-1}$; 43 soundings). In both sets of profiles, there is the indication of a boundary layer having a structure similar to that described above. Below approximately 900 mb the moist potential temperatures are relatively well-mixed before increasing more sharply with altitude above this level. The boundary layer depth appears to be similar for both the rising and the sinking regimes. Relative humidity also decreases with altitude, though the troposphere in the rising motion composite is more humid at all levels (recall Fig. 5d). Consistent with the argument that the vertical velocity influences C_s by controlling cloud formation above the boundary layer, mean C_s for the rising composite is -150.7 $W\,m^{-2}$, while mean C_s for the sinking composite is -109.2 $W\,m^{-2}$.

Let us briefly revisit the question of radiative forcing due to low clouds alone. As we have discussed previously (and inferred from Fig. 4), the con-

tribution to total column C_s from low-level clouds can approach -100 $W\,m^{-2}$ during the summertime. However, our discussion of low-level cloud cover and cloudy boundary layers indicates that clouds which form beneath an inversion during summertime are only a few hundred meters thick. Is it reasonable to assume that this cloud layer is sufficient to produce the observed degree of radiative forcing? During July, daily-mean insolation in the NH midlatitudes is approximately 400 $W\,m^{-2}$ (e.g. see Fig. 6.4 in Peixo and Oort, 1992). Therefore, a cloudy to clear-sky albedo difference of 25% is sufficient to produce a C_s value of -100 $W\,m^{-2}$. Since, in the latitude range 40-60°, clear-sky albedo over the oceans is approximately 15–20% (Harrison et al., 1990), a total albedo of approximately 40–45% would result in a summertime C_s on the order of -100 $W\,m^{-2}$.

We can calculate the approximate liquid-water content (LWC) for a marine stratiform cloud in the following way (Liou, 1992):

$$LWC \approx \frac{4}{3}\pi R^3 N \rho_l \ . \tag{3}$$

R is the mean droplet radius weighted by the droplet size distribution, N is the total droplet number concentration, and ρ_l is the density of liquid water. From Table 4.2 and Fig. 4.10 in (Liou, 1992), we find that, for low-level marine stratus, droplet radius ranges from approximately 2 to 12 μm. N can take on a wide range of values from 50 to 1000 cm^{-3}, but a typical value for low-level oceanic clouds is approximately 100–200 cm^{-3} (Liou, 1992; Pruppacher and Klett, 1978). Choosing a value of 7 μm for R, and using $N = 150\ cm^{-3}$, we calculate a LWC of approximately 0.2 $g\,m^{-3}$. Cloud albedo is actually related to liquid-water path (LWP), rather than LWC, and LWP is approximately defined as (Liou, 1992):

$$LWP \approx LWC \cdot \Delta z \ . \tag{4}$$

Δz represents the cloud thickness. For a typical cloud thickness of 300 meters, LWP is calculated to be 60 $g\,m^{-2}$. From Liou (1992) and Stevens and Webster (1981), we find that this LWP corresponds to a cloud albedo (for plane-parallel clouds) in the range 50-70% for a variety of solar zenith angles. Therefore, consistent with the observational findings, low-level cloud of a few hundred meters thick and a cloud fraction of about 60% should be able to contribute significantly to C_s.

By contrast, observations of cirrus clouds have shown that typical ice-water content (IWC) of these clouds is often on the order of 0.01 to 0.1 $g\,m^{-3}$ (Liou, 1992). A simple calculation similar to the one above leads to the conclusion that a few hundred meter thick boundary layer cloud can have the same influence on C_s as a several kilometer thick upper-level cloud. Another point to consider is that, while the C_s magnitude of thick middle and

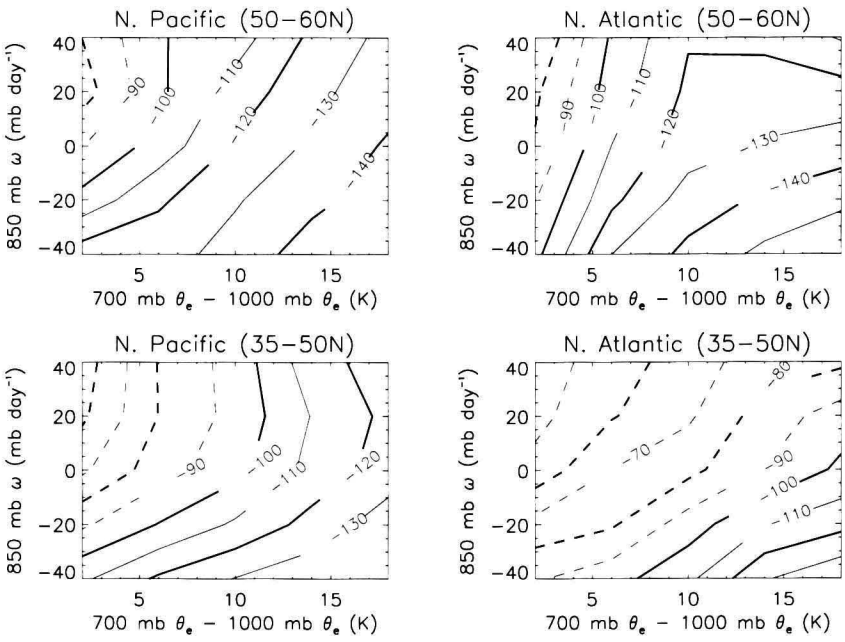

Fig. 10. Phase diagram of C_{sn} as a function of vertical velocity and static stability.

high clouds can be large, C_l is also larger than for boundary layer clouds, reducing the net radiative effect at the top of the atmosphere. It is difficult to overstate the importance of low clouds in the Earth's shortwave and net radiation budget.

5 Regional and seasonal CRF variations

Now we are in a position to examine the regional and seasonal CRF variations based on the variation of two parameters; vertical velocity and static stability. Fig. 10 shows a phase diagram of daily-mean C_{sn} as a function of daily-mean 850 $mb\ \omega$ and $700\,mb\,\theta_e - 1000\,mb\,\theta_e$ in the North Pacific and North Atlantic for the period July 1985-89. C_{sn} clearly varies in conjunction with both parameters such that regimes characterized by rising motion ($\omega < 0$) and large values of this index of static stability have the most highly reflective clouds, and vice versa. An equivalent diagram for January shows similar characteristics.

Moving to longer timescales, we recall from Table 1 that monthly-mean cloud cover increases from winter to summer in the North Pacific and decreases from winter to summer in the North Atlantic. C_{sn} displays similar behavior. Consistent with our understanding of the variation of C_{sn} as a func-

Table 3. Variation of C_{sn} with ω variance and static stability and contribution of dynamical vs. boundary layer clouds to total C_{sn}.

	N. Pacific		N. Atlantic	
Parameter	Jan	Jul	Jan	Jul
C_{sn} $(W\,m^{-2})$	-114	-121	-109	-86
500 mb $([\omega\prime^2])^{1/2}$ $(mb\,day^{-1})$	144.2	65.9	132.3	61.2
$700\,mb\,\theta_e - 1000\,mb\,\theta_e$ (K)	3.4	16.0	3.6	9.5
Cloud type				
BL C_{sn} as % of total	34	65	34	63
Dyn C_{sn} as % of total	66	35	66	37

tion of ω and static stability, and following the discussion in Weaver and Ramanathan (1997), Table 5 shows mean values of C_{sn}, 500 mb ω variance, and $700\,mb\,\theta_e - 1000\,mb\,\theta_e$ for January and July 1985-89 (the regions represented are the same as in Table 1). The ω variance in Table 5 is defined as $([\omega\prime^2])^{1/2}$, where $\omega\prime$ represents the daily deviation from the monthly-mean ω value and the square brackets represents averaging over the month. Since CRF increases with increased rising motion, but doesn't decrease with increased sinking motion (recall Fig. 4), increases in ω variance should lead to increases in CRF. For monthly-mean comparisons, some measure of ω variance is more useful than monthly-mean ω, because simply averaging over many rising and sinking events at a given point would lead to a mean ω value close to zero (Weaver and Ramanathan, 1997). For these purposes, ω variance can be considered as an indicator of synoptic-scale activity (e.g. cyclone frequency and intensity), which tends to force enhanced cloud formation above the boundary layer. During July, while ω variance is approximately the same in the North Atlantic as in the North Pacific, the North Pacific is significantly more stable, and hence has greater low-level cloud cover (recall Table 3) with a greater total C_{sn} magnitude. During January, both static stability and ω variance are approximately the same in the North Pacific and North Atlantic, and therefore cloudiness and C_{sn} are also approximately the same. In the North Pacific, while synoptic activity is greatly enhanced during January (ω variance is a factor of two greater), static stability is much greater during July, and the resulting large increase in low-level cloud cover seems to outweigh the contribution of clouds forced by large-scale rising motion above the boundary layer. By contrast, in the North Atlantic, the seasonal change in ω variance is approximately the same as in the North Pacific, but the summertime increase in static stability is significantly less pronounced, leading to smaller mean cloud cover and C_{sn} during July.

As pointed out throughout this paper, our conceptual model of CRF

over extratropical oceans considers two general cloud types; boundary layer clouds whose forcing depends primarily on static stability, and middle and high clouds which depend on large-scale vertical velocity in the free troposphere associated with synoptic-scale dynamics such as cyclones. A useful exercise is to use this understanding in order to attempt to separate the effect of both types of clouds on the monthly-mean radiation balance at the top of the atmosphere. We have used a numerical radiative transfer model, initialized with mean July extratropical North Atlantic temperature and humidity profiles, in order to calculate C_l for optically thick low-level clouds. We find that clouds with tops between approximately 850 and 750 mb have C_l values in the range 5-10 $W\,m^{-2}$. Limiting our C_{sn} sample (for the North Atlantic during July 1985-89) to those points which have C_l values less than 10 $W\,m^{-2}$, we are able to calculate a linear regression of C_{sn} with low-level $\Delta\theta_e$ (between 700 and 1000 mb) as a rough estimate for the dependence on static stability of the C_{sn} of low clouds. Therefore, knowing the θ_e difference and total C_{sn} at each point, we can subtract the contribution to C_{sn} due to low clouds, and the remainder is the contribution from middle and high clouds arising from synoptic-scale rising and sinking motions.

We can apply this regression to different regions and seasons. Table 5 summarizes the relative proportions of 'boundary layer C_{sn}' (BL C_{sn}) and 'dynamical C_{sn}' (Dyn C_{sn}) in the North Pacific and North Atlantic during January and July. As we might expect, the contribution from Dyn C_{sn} to total C_{sn} is much greater during January than July in all regions considered, reflecting the more intense synoptic activity during winter. During summer, however, the reverse is true, with BL C_{sn} contributing the greater percentage due to the decrease in cyclone frequency and intensity and the increase in low-level static stability. Thus, boundary layer clouds are the most important contributor ($> 60\%$) to C_s during a season (summer), and in a region (NH extratropical oceans), dominant in the global radiation balance.

6 Summary and Discussion

Drawing on the recent studies summarized here, we can ask the question, why is CRF in the NH oceanic storm tracks so large, and what controls its variability? Several cooperative factors contribute to this large CRF: Extensive cloud cover is typically present at many levels of the atmosphere, from boundary layer clouds to middle and high clouds. In the free troposphere, large-scale vertical circulations associated with storm track dynamics help control the formation or suppression of mid- and upper-level clouds. Boundary layer clouds are prevalent under most conditions, and their coverage seems to be a strong function of the lower-tropospheric static stability.

To first order, we are able to explain regional and seasonal variations in CRF as a function of variations in two parameters; vertical velocity and

static stability. For example, July-mean C_{sn} is greater in the North Pacific relative to the North Atlantic because, while vertical velocity variance is similar, low-level static stability is much greater in the North Pacific (Table 5). During January, both vertical velocity and static stability are similar in the North Pacific and North Atlantic, and therefore C_{sn} and total cloud cover is approximately the same. Seasonally, C_{sn} magnitude is greater in the North Pacific during July than January because the summertime increase in static stability, and corresponding increase in low-level cloud fraction, counteracts the increased wintertime storm track activity. Since the static stability increase from winter to summer is much smaller in the North Atlantic, the effect of vertical velocity variance appears to dominate, leading to greater wintertime cloud cover and CRF.

There are many unanswered questions and requirements for continued research. First, while there is a clearly-demonstrated link between low-level static stability and low cloud fraction, the physics which underlies the correlations from climatological observations is less well-understood. Previous studies have indicated that boundary layer cloud tops can be unstable to mixing with air above the boundary layer, and that this instability tends to increase as static stability decreases (Randall, 1980; Deardorff, 1980b). Attempts to parameterize cloud fraction by theoretical measures of this instability criterion have met with mixed success, however e.g. see Albrecht et al. (1995b), and additional study is necessary in order to obtain a physically-based understanding of what controls boundary layer cloud fraction and other properties. In addition, while cyclones and synoptic-scale disturbances have a clear effect on the vertical velocity field, we have not examined their role in influencing low-level static stability and other boundary layer properties (such as depth and humidity) with the potential to influence low-level cloud cover. This also requires further investigation.

One ultimate goal of the type of study summarized in this paper is to address questions relating to the prediction of climate change. As stated in the introduction, the role of clouds and cloud processes in influencing climate change has yet to be adequately quantified. Comparison of these types of cloud observations and statistics with the current generation of state-of-the-art climate models can help provide more accurate and realistic parameterizations of model clouds and hence lead to simulations which further our understanding of cloud-climate feedbacks. As discussed in this paper, clouds over the extratropical ocean regions have a strong impact on the net radiation balance. In particular we have identified boundary layer clouds as being key contributors to the total column CRF (recall Table 5). As such, understanding what controls the coverage and properties of these clouds, as well as their interactions with the highly dynamical environment of the extratropical regions, is a key area of study in climate and global change science.

Acknowledgement

The authors gratefully acknowledge the support and invitation to participate in this Colloquium from the Royal Netherlands Academy of Arts and Sciences. We also appreciate the organizational and editorial skills of Bert Holtslag and Peter Duynkerke. The authors' research has been supported by NASA CERES NAG 1-1259 and the NSF Center for Clouds, Chemistry and Climate (C^4) ATM 94-05024. This paper is C^4 publication number 183.